Review of a simple noise simulation technique in digital radiography

doi: 10.1007/s12194-012-0152-7

Title

Review on simple noise simulation technique in digital radiography

Authors * Corresponding author

Rie Tanaka, Katsuhiro Ichikawa, Kosuke Matsubara, Hiroki Kawashima

Affiliation

[1] School of Health Sciences, College of Medical, Pharmaceutical and Health Sciences, Kanazawa University; 5-11-80 Kodatsuno, Kanazawa, 920-0942 Japan

[2] Department of Radiology, Kanazawa University Hospital; 13-1 Takara-machi, Kanazawa, 920-8641, Japan

Telephone and Fax numbers and E-mail Address of Corresponding Author

Rie Tanaka, PhD

Tel: +81-76-265-2537

Fax: +81-76-234-4366

E-mail: rie44@mhs.mp.kanazawa-u.ac.jp

Department of Radiological Technology, School of Health Sciences, College of Medical, Pharmaceutical and Health Sciences, Kanazawa University; 5-11-80 Kodatsuno, Kanazawa, 920-0942, Japan

Key words: noise simulation, image quality, exposure dose, digital radiography, flat panel detector (FPD)

Review on simple noise simulation technique in digital radiography

Abstract

Reduction of exposure dose and improvement in image quality can be expected to result from advances in the performance of imaging detectors. A number of researchers reported on methods for simulating reduced dose images. The simplest method provides reduced dose images by adding white Gaussian noise with certain standard deviation to the original image. The aim of this paper was to develop and validate a fundamental system with a graphical user interface for simulating reduced-dose images by the simple method. Here, we describe a technical approach in a flat-panel detector (FPD) system and validate the simulation performance objectively and subjectively. Additionally, the technical limitations and possible solutions are suggested based on the

validation results in this paper.

Key words: noise simulation, image quality, exposure dose, digital radiography, flat panel detector (FPD)

Introduction

Digital X-ray imaging systems have been commonly used in place of analog systems in clinical practice. A reduction of the exposure dose and improvement in image quality can be expected to result from advances in the performance of imaging detectors. In a conventional analog system, imaging conditions needed to be adjusted to provide the necessary film density. In contrast, in a digital system, the image quality is assured to some extent by post image processing even if the imaging was not performed under appropriate conditions. That is, it is necessary to have the concern about imaging conditions more than in an analog imaging system to avoid an excessive patient dose. In general, imaging conditions are customized empirically by trial and error on the basis of general parameters, radiation measurements, and image observations in each institution. However, it is too complicated to verify imaging conditions in various part of body by such an approach in daily clinical practice. Although there is another approach to determining imaging conditions based on experience and intuition, it is discouraged because of a lack of evidence for decision.

An alternative is simulation of the effect of dose reduction on image quality. A number of researchers reported on methods for simulating reduced dose images. Such techniques have been applied in computed radiography (CR) [1], digital radiography (DR) [2, 3], and computed tomography (CT) [4-6]. Bath et al. developed an accurate simulation method for CR system. The method uses information about noise power spectrum (NPS) and detective quantum efficiency (DQE). This method is well-established for reduced-dose simulation, however, requires specialized equipment to measure DQE and NPS. In addition, the correction for differences in DQE over the dose variations remains to be incorporated. Veldkamp et al. developed a technique for simulating the effect of dose reduction on image quality for DR system. The technique provides reduced dose images by adding white Gaussian noise with certain standard deviation to the original image, similar to noise simulation techniques used for CT [4-6]. Frequency dependency of noise power in reconstructed CT images is mainly the results of the filtered back projection. The frequency dependency of noise power in raw CT data is, therefore, of less importance. Thus, the simplified method could be acceptable for simulating reduced-dose images in CT. However, there is a limitation to simulate image noise with high accuracy in digital radiography images. This is because unknown relation between spatial frequency and noise may affect the visual appearance and detectability.

Even though there are technical limitations in the simplified method, it is still advantageous in daily clinical practice. It would be beneficial to review the basic and

simple simulation technique to develop an improved method. The aim of this paper was to develop and validate a fundamental system with a graphical user interface (GUI) for simulating reduced-dose images by the simple method. Here, we describe a technical approach in a flat-panel detector (FPD) system and validate the simulation performance objectively and subjectively. Additionally, the technical limitations and possible solutions are suggested based on the validation results in this paper.

1. Materials and methods

1-1 Imaging system

An indirect-type (CsI) flat-panel detector (FPD) system (PLAUDR C50, Konica Minolta, Japan) with an X-ray generator (UD150L-40E, Shimadzu, Japan) was used in this study. The matrix size was 3072×3072 pixels, the pixel size was 0.139×0.139 mm, and the field of view was 43.2×43.2 cm. The pixel scaling was linear with respect to exposure, with a bit depth of 12 bits. All measurements were conducted without grid in front of the detector. Image preprocessing consisted of offset and gain correction as well as compensation for defective or nonlinear pixels, as applied in normal clinical use of the detector.

1-2 Development environment

Our prototype system was developed on a personal computer (CPU, Pentium 4, 2.6 GHz; Memory, 2 GB; operating system, Windows XP; Microsoft, Redmond, WA) (Development environment, C++Builder; Borland, Scotts Valley, CA).

1-3 Measurement of input-output characteristics

An RQA5 X-ray spectrum was used (HVL=7.1 mm Al, realized with 21 mm Al additional filtration at 74 kV) for determination of input-output characteristics according to IEC61267 [7] and IEC62220-1 [8]. The air kerma values were measured free-in-air in the detector plane with an ionization chamber (AE-132a 2902209; Oyogiken Inc., Tokyo, Japan). The source-to-image distance (SID) was limited to 1.5 m in the system evaluated. The ionization chamber was placed 500 mm behind the detector. The exposure dose was measured from 0.5 mAs to 120 mAs, and images were obtained. The air kerma at the detector surface was calculated by the inverse-square distance law. The measurements were performed three times at each dose level, and the average air kerma was calculated. Regions of interest (ROIs) were located manually near the detector center on images, 100×100 pixels in size, and average pixel values were measured with Image-J ver. 1.42 (http://rsb.info.nih.gov/ij/) in each ROI.

Input-output characteristics were plotted so that the linearity between the exposure dose and pixel values was confirmed.

1-4 Creation of conversion function from pixel value to quantum number

Quantum noise is linearly related to the square root of the absorbed dose in the detector, and the raw pixel values are proportional to the detector dose in linear system. Consequently, the quantum noise is proportional to the square root of the pixel values. However, in this study, the relationship between pixel values, exposure dose, quantum number was addressed to create a conversion function for better understanding of the present method and for the future extensibility.

The exposure dose measured at the detector surface (C/kg) was converted to absorbed dose (Gy). The incident quantum number q to the detector per pixel (counts/pixel) was calculated according to the pixel size of the detector (0.139 mm) and the quantum number in RQA5, 30174 ($1/mm^2/\mu Gy$), determined in IEC62220-1 [8]. The relationship among the tube current-time product (mAs), exposure dose (C/kg) at the detector surface, the number of incident quanta (count/pixel), and pixel values measured on the images was addressed, and a conversion function was then created by fitting of the results to a linear function, $y=a+bx$. In addition, the incident quantum numbers through the object (acrylic plate, thickness; 15 mm, density; 1.19 g/cm^3, attenuation coefficient; 2.07×10^{-2} m^2/kg) was also calculated from $I=I_0 \cdot e^{-\mu x}$ (I_0: incident quantum number, I: incident quantum number at a depth of x m, μ: linear attenuation coefficient), and the conversion function for imaging an object was created as well [9,10].

1-5 Simulation of image noise

Image noise was induced by statistical fluctuation of the quanta incident to the detector, which followed a Poisson distribution. Thus, for simulation of image noise, the map of incident quantum numbers was input into the Poisson random-number generator in each pixel [11, 12].

First, the image obtained at 63 mAs just before the pixel values became saturated was used as an input image to our simulation system. In this study, it was 63 mAs (100 mA, 630 msec, SID=150 cm) at the exposure quality of RQA5. Second, the image was converted into a map of incident quantum numbers by use of the conversion function as shown in Fig. 1. The incident quantum numbers were changed by multiplying the map by a weighting factor from 0.1 to 1.0, in increments of 0.1, in each pixel for simulation of images at various noise levels. Finally, each pixel in the weighted map

was input into the random-value generator. The output values from the random number generator were again converted into pixel values through the conversion function. The final output image was noise simulation image. Figure 2 shows the output images, histograms, and NPS resulting from input pixel values of 10, 100, and 1000. We confirmed that the NPS became 1/10 with tenfold increase in input pixel value.

1-6 Validation of the developed system

For ensuring the consistency between simulation and actual images, simulation images were compared with actual images provided by use of the FPD system at different noise levels of 0.85×10^{-7} C/kg (0.33 mR), 2.84×10^{-7} C/kg (1.06 mR), and 8.02×10^{-7} C/kg (3.11 mR). In this study, the developed system was examined under fixed conditions of 74 kV (RQA5) and SID=150 cm.

1-6-1 Objective evaluation

The NPS was measured in the simulation flat-field images and compared with those of the actual flat-field images at the three different dose levels mentioned above.

Three independent flat-field images were obtained with use of the RQA5 X-ray spectrum (74 kV, 100 mA, SID=150 cm) at each of three exposure levels. ROIs were located manually near the detector center, 256×256 pixels in size, and the average pixel values were measured in the ROIs. The results were 120, 1167, and 4797, respectively. They were converted to the quantum numbers, 448, 4332, and 17807, respectively, by use of the conversion function (as results of y=0.2694x+100) as shown in Fig. 1. The quantum numbers were input into a random-number generator for creation of simulation images at each noise level.

The NPS was calculated according to IEC62220-1 [8]. To remove long-range background trends, a two-dimensional 2^{nd} order polynomial was fitted to each image and subtracted from each image. The 2-D NPS was then calculated by applying the fast Fourier transform to each ROI. One-dimensional cuts through the 2-D NPS were obtained by averaging of the central ± 7 lines (excluding the axis) around the horizontal and vertical axes. We input the quantum numbers into the simulation system to simulate image noise. To facilitate the comparison in the actual and simulation images at each dose level, NPS was averaged using the results from 0.14 to 3.5 [cycle/mm] in each exposure level.

1-6-2 Subjective evaluation

An observer study was conducted to ensure the visual consistency between the simulated and actual images by six radiological technologists with 1~10 years experience. Images of barger phantom (acrylic plate with concave ditches, thickness; 15 mm, ditch diameter; 0~10 mm, ditch depth; 0.5~10mm) were obtained at the three exposure dose levels. In addition, an image of the barger phantom was obtained at the exposure level at which the pixel values become saturated, 18×10^{-7} C/kg (6.96 mR), to be used as an input image into the simulation system. Simulation images were provided by inputting of the image into the conversion function (y=0.3706+100) and random number generator. The actual and simulation images had almost the same average pixel value and standard division. To adjust visual appearance, the window level and width of the images were adjusted to the average pixel value of the images and double the window level, respectively, and the adjusted images were saved in BMP format. A pair of actual and simulation images were prepared at three exposure levels. They were displayed on a 2M monochrome liquid crystal display (LCD) (RadiForce GS220, EIZO, Japan) and compared in terms of the detection of signals in the barger phantom images. Observers determined signals which could be detected with a confidence of 50 %. The observation distance and time were set depending on each observer; however, the room brightness was maintained at 50 lx. The minimum diameter and depth of the ditch were determined, and contrast- detail (C-D) curves were created at each exposure dose level. Image noise affects the visual appearance and detectability of an object with low contrast. Thus, subjective validation was performed based on image quality figures (IQF). Image quality figures were calculated based on the resulting C-D curves [13]. The IQF is the integration of the minimum diameter of the signal at each contrast and is calculated as follows;

$$IQF = \frac{n}{\sum_{i=1}^{n} C_i \cdot D_{i.\min}} \qquad (1),$$

where *Ci*, *Di*, and n are the depth and diameter of each ditch, and the number of steps, respectively. A larger IQF means better image quality. Paired t-test was performed to evaluate the differences between the IQF of the actual and simulation images in each exposure level.

1-7 Association of image quality with exposure dose

We created look-up table (LUT) to associate the pixel value with the exposure dose by using the conversion function as shown in Fig. 1. The LUT was installed in the simulation system with a GUI which indicates the necessary exposure dose (mR) and

tube current-time product (mAs) to provide the necessary image quality in diagnosis. In this preliminary study, the simulation system was designed under restricted conditions of 74 kV (RQA5) tube voltage and 15 mm object thickness.

2. Results

2-1 Objective evaluation

Figures 3 shows average NPS level of the actual and the simulation image at each exposure, respectively. The average NPS of the actual image at each dose level were 3.75×10^{-5}, 6.77×10^{-6}, and 4.90×10^{-6}, and those of the simulation image were 4.41×10^{-5}, 4.53×10^{-6}, and 1.10×10^{-6}. The average NPS decreased as the exposure dose increased both in the actual and in the simulation images. In addition, they indicated almost the same average NPS at the same dose level. However, NPS of the actual images varied with spatial frequencies, while, NPS of the simulation images were stable throughout spatial frequencies. Figure 4 shows NPS of the actual and simulation images at 1.06 mR. In the actual image, NPS showed slightly lower noise levels for higher spatial frequencies and slightly higher noise levels for lower spatial frequencies.

2-2 Subjective evaluation

Figure 5 shows the actual and simulation images of burger phantom. In an observer study, both images showed almost the same signal detectability, which decreased with decreasing exposure dose. Figure 6 shows the average IQF for 6 observers, calculated from C-D curves. There was no significant difference between the actual images and the simulation images at the same exposure dose level ($P<0.01$). Figure 7 shows enlarged holes in the image of burger phantom. As shown in Fig. 7, the simulated images had quite similar appearance as compared to the actual dose images.

2-3 Estimation of exposure dose

Figure 8 shows the GUI of the system we developed. The GUI was very useful for observation of images with interactively changing image noise levels and exposure dose levels.

3. Discussion

We developed a noise simulation system with GUI for simulating reduced-dose images by adding white noise to the original image. The technique was validated objectively and subjectively. Comparable noise level and detection performance were shown in the actual and simulation images. In addition, the simulation system with the GUI was

useful for observing images with changing image noise and exposure dose levels. We confirmed that the method would give promising results for simulating image noise under different dose levels.

Some technical issues should be taken in consideration. The noise in the images is not solely quantum limited, and the other noise factors are thought to be the cause of change in NPS throughout spatial frequencies. In contrast, simulation images had almost the same NPS throughout spatial frequencies in the actual images. These results indicated that simulation images could not simulate the other noise factors, such as electrical noise and structural noise, which were involved in the actual images. This is the technical limitation of this simple simulation approach, as reported by the investigators [1,2]. However, significant differences in visual appearance were not observed between the actual and simulation images in this study. Our results are supported by the results in the previous research describing that the appearance of noise and low-contrast objects appeared visually comparable for a human observer [2]. These results mentioned that the presented simplified technique seems sufficient for investigating trends in image quality as a function of dose reduction.

However, for creating fully-simulated image noise, it is necessary to correct the influence of those factors varying with spatial frequency. This is a major challenge for this approach. One of the solutions is creating the conversion function considering the variations of NPS over spatial frequency. However, it is a tough work to create such an ideal function because of requiring an enormous quantity of data. For clinical implementation, it is crucial to have corporations from manufacturers and to simplify the procedures by installing the conversion function as initial data at the system installation.

4. Conclusion

We developed and validated the fundamental system with GUI for simulating reduced-dose images by adding white noise to the original image. Simulation images were compared with the actual images physically and visually, and the consistency between them was confirmed. The results identified the characteristics of conventional but promising simulation technique. For development of practical system, the leading challenge is to correct for variations of NPS with spatial frequency. The next step is to create the conversion function considering the noise properties.

Acknowledgments

This work was supported in part by a research grant from the Japanese Society of

Medical Physics (JSMP).

References

[1] Båth M, Håkansson M, Tingberg A, Månsson LG. Method of simulating dose reduction for digital radiographic systems. Radiat Prot Dosimetry. 114(1-3):253-9, 2005

[2] Veldkamp WJ, Kroft LJ, van Delft JP, Geleijns J. A technique for simulating the effect of dose reduction on image quality in digital chest radiography. J Digit Imaging. 22(2):114-25, 2009

[3] Saunders RS Jr, Samei E. A method for modifying the image quality parameters of digital radiographic images. Med Phys. 30(11):3006-17, 2003

[4] van Gelder RE, Venema HW, Florie J, Nio CY, Serlie IW, Schutter MP, van Rijn JC, Vos FM, Glas AS, Bossuyt PM, Bartelsman JF, Laméris JS, Stoker J. CT colonography: feasibility of substantial dose reduction--comparison of medium to very low doses in identical patients. Radiology. 232(2):611-20, 2004

[5] van Gelder RE, Venema HW, Serlie IW, Nio CY, Determann RM, Tipker CA, Vos FM, Glas AS, Bartelsman JF, Bossuyt PM, Laméris JS, Stoker J. CT colonography at different radiation dose levels: feasibility of dose reduction. Radiology. 224(1):25-33, 2002

[6] Frush DP, Slack CC, Hollingsworth CL, Bisset GS, Donnelly LF, Hsieh J, Lavin-Wensell T, Mayo JR. Computer-simulated radiation dose reduction for abdominal multidetector CT of pediatric patients. AJR Am J Roentgenol. 179(5):1107-13, 2002

[7] International electrotechnical commission, IEC International standard 61267 Medical diagnostic X-ray equipment-Radiation conditions for use in the determination of characteristics. Geneva, Switzerland: IEC, 1994

[8] International electrotechnical commission, IEC International standard 62220-1. Medical diagnostic X-ray equipment-Characteristics of digital imaging devices-Part 1: Determination of the detective quantum efficiency. Geneva, Switzerland: IEC, 2003

[9] International commission on radiation unit and measurement (ICRU). Tissue substitutes in radiation dosimetry and measurement. ICRU report 44, Bethesda, MD, USA: ICRU, 1989.

[10] Brandrup J, Immergut EH, and Grulke EA. Polymer handbook (4th edn), New York, USA: Wiley-Interscience, 2003.

[11] Dainty JC, and Shaw R. Image Science. London, UK: Academic Press, 1974

[12] Walter H. Review of radiologic physics (3rd edn), Philadelphia, USA: Lippincott

Williams & Wilkins, 2010
[13] Samei E, Hill JG, Frey GD, Southgate WM, Mah E, Delong D. Evaluation of a flat panel digital radiographic system for low-dose portable imaging of neonates. Med Phys. 30(4):601-7, 2003

Figure legends

Figure 1 Relationship among tube current-time product (mAs), exposure dose (C/kg) at the detector surface, the quantum number per pixel (count/pixel), and pixel values measured on images obtained (RQA5 X-ray spectrum of HVL=7.1 mm Al, with 21 mm Al additional filtration at 74 kV in SID=150cm). The thick and fine lines represent conversion functions without and with an acrylic plate, respectively.

Figure 2 Output images from random-value generator, histograms, and noise power spectrum (NPS) obtained by inputting pixel value (a) 10, (b) 100, and (c) 1000.

Figure 3 Average noise power spectrum (NPS) of the actual and simulation images at each exposure level

Figure 4 Noise power spectrum (NPS) of (a) the actual and (b) simulation images at 2.84×10^{-7}C/kg (1.06mR)

Figure 5 Barger phantom images provided by the FPD system (Upper) and simulation system (Lower) at the exposure dose of (a) 0.85×10^{-7}C/kg (0.33 mR), (b) 2.84×10^{-7}C/kg (1.06mR), and (c) 8.02×10^{-7}C/kg (3.11mR)

Figure 6 Comparison of IQF calculated from contrast-detail curves for actual images and simulation images. (n=6)　Error bars show +/-SD.

Figure 7 Zoomed detail of one of the holes in (a) the actual and (b) simulation images of burger phantom.

Figure 8 Graphical user interface (GUI) of our system (Upper) and simulation images (Lower). The percentages show incident quantum number (%) relative to the base image, *i.e.*, when a map of incident quantum numbers is multiplied by a weighting factor of 0.1, incident quantum number (%) becomes 10%.

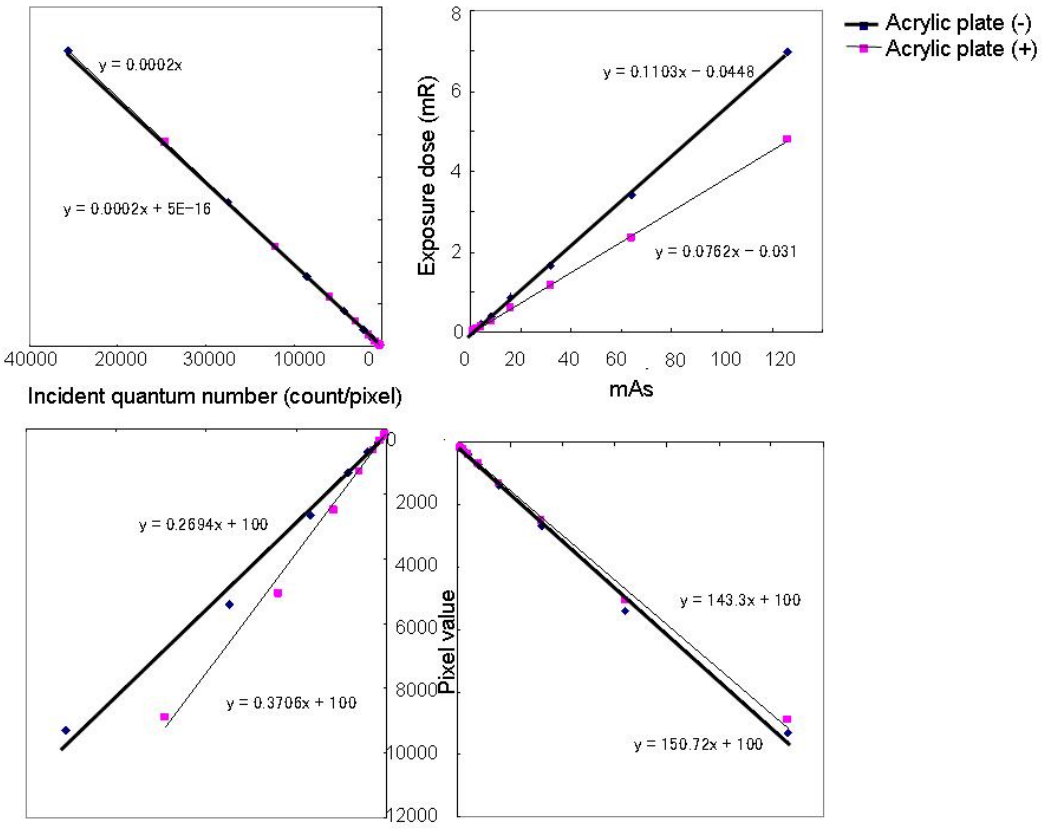

Figure 1 Relationship among tube current-time product (mAs), exposure dose (C/kg) at the detector surface, the quantum number per pixel (count/pixel), and pixel values measured on images obtained (RQA5 X-ray spectrum of HVL=7.1 mm Al, with 21 mm Al additional filtration at 74 kV in SID=150cm). The thick and fine lines represent conversion functions without and with an acrylic plate, respectively.

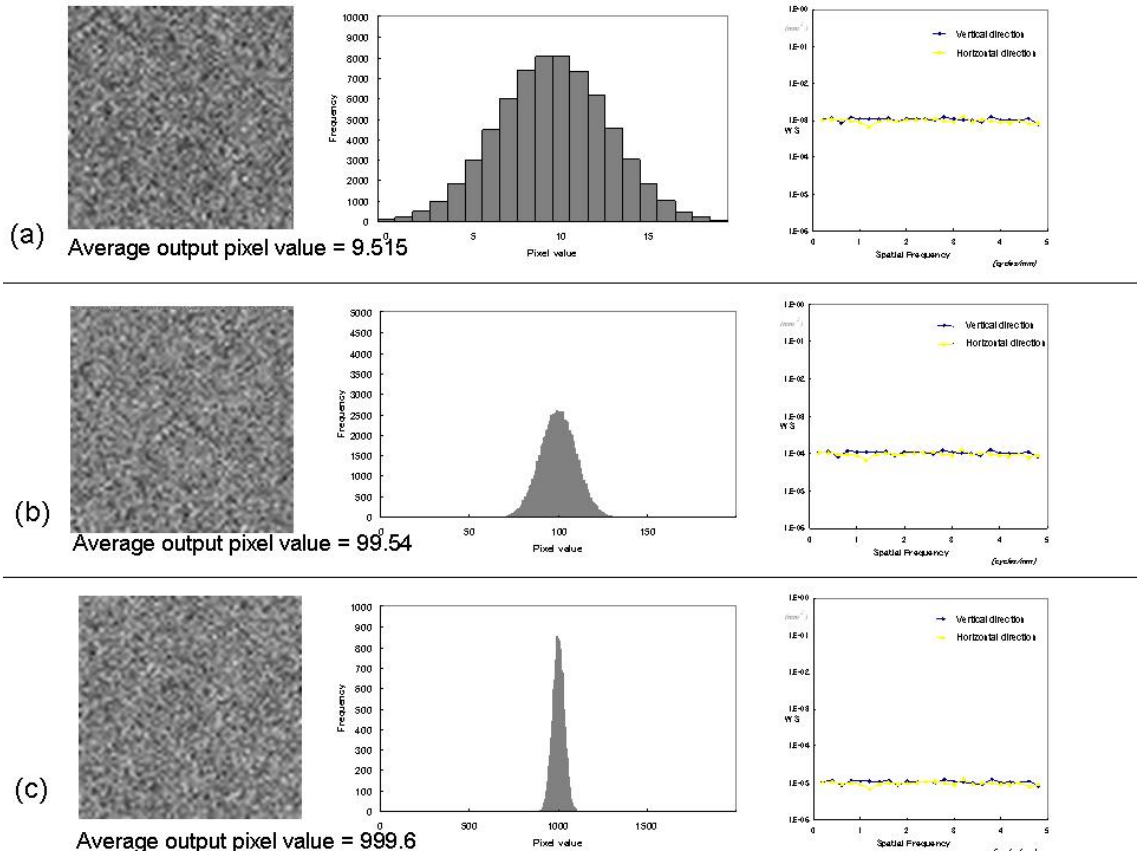

Figure 2 Output images from random-value generator, histograms, and noise power spectrum (NPS) obtained by inputting pixel value (a) 10, (b) 100, and (c) 1000.

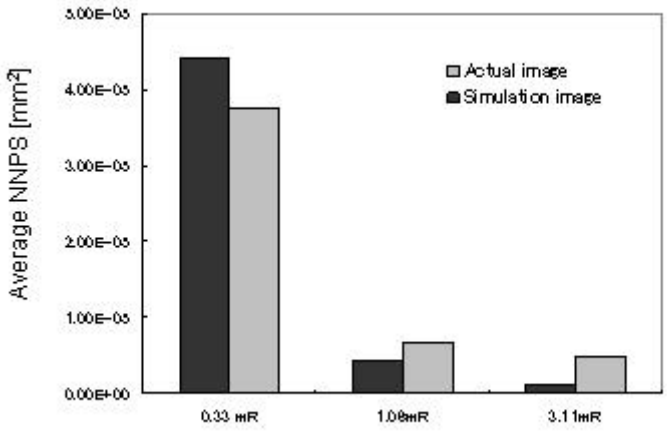

Figure 3 Average noise power spectrum (NPS) of the actual and simulation images at

each exposure level

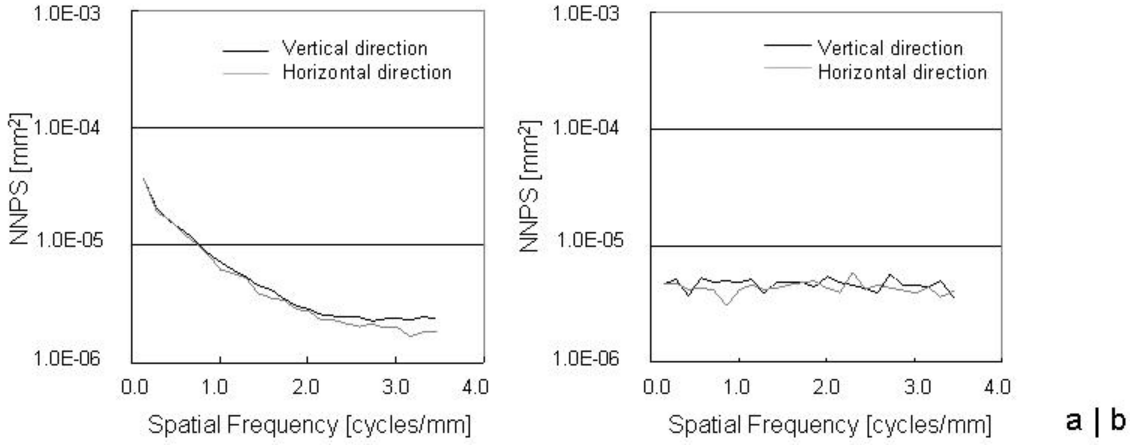

Figure 4 Noise power spectrum (NPS) of (a) the actual and (b) simulation images at 2.84 $\times 10^{-7}$C/kg (1.06mR)

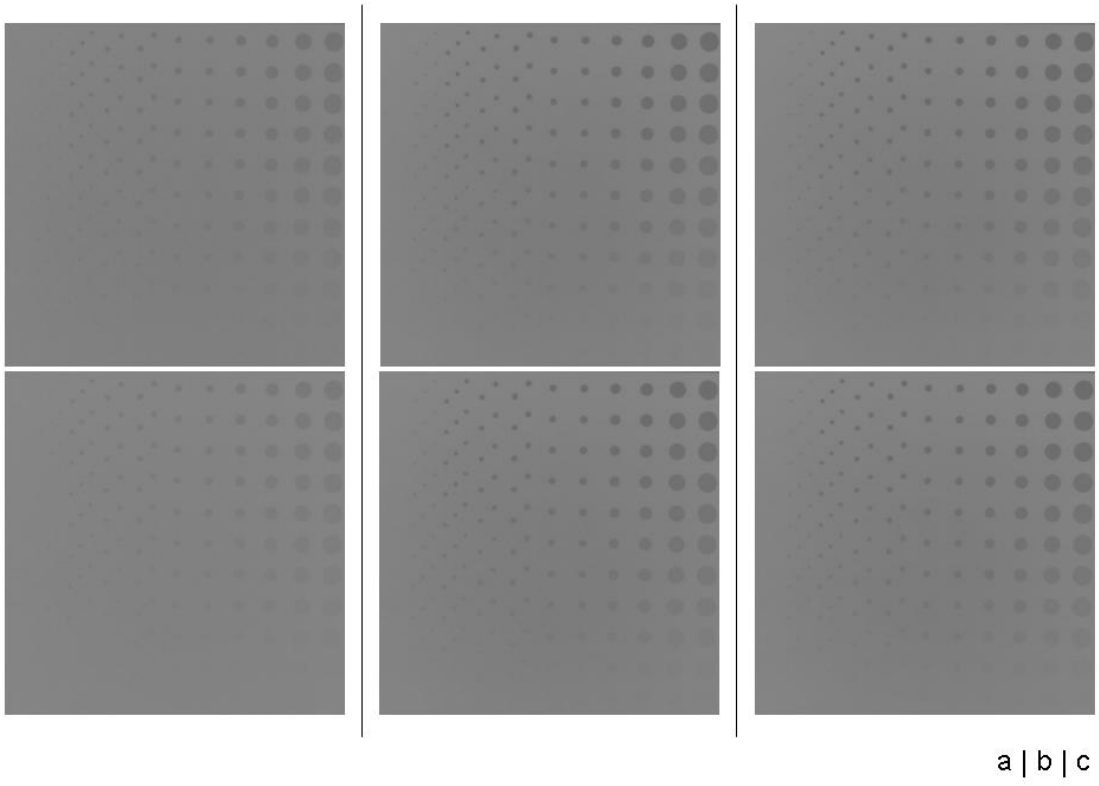

Figure 5 Barger phantom images provided by the FPD system (Upper) and simulation system (Lower) at the exposure dose of (a) 0.85×10^{-7}C/kg (0.33 mR), (b) 2.84×10^{-7}C/kg (1.06mR), and (c) 8.02×10^{-7}C/kg (3.11mR)

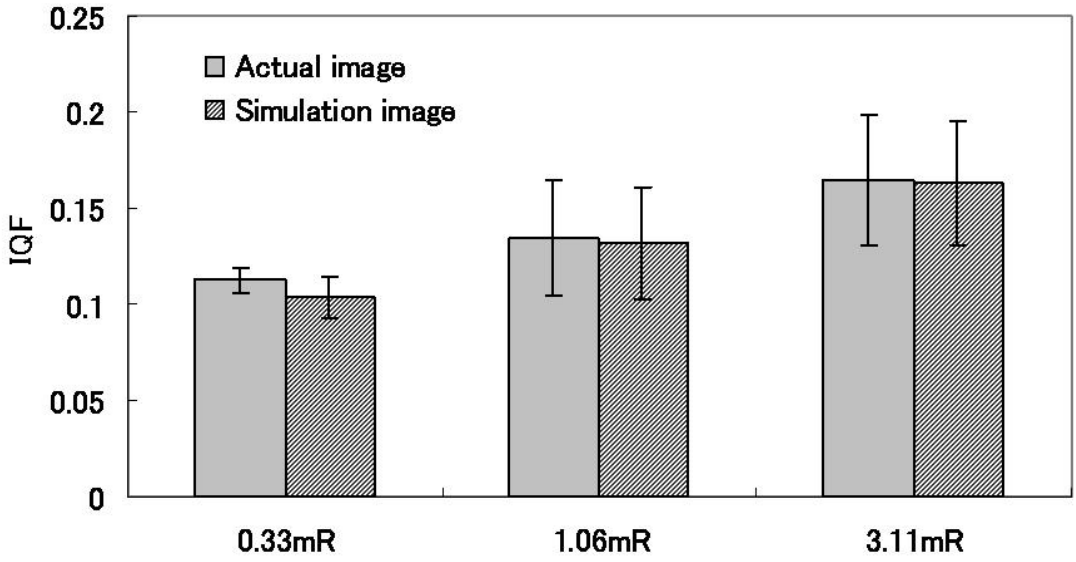

Figure 6 Comparison of IQF calculated from contrast-detail curves for actual images and simulation images. (n=6)　Error bars show +/-SD.

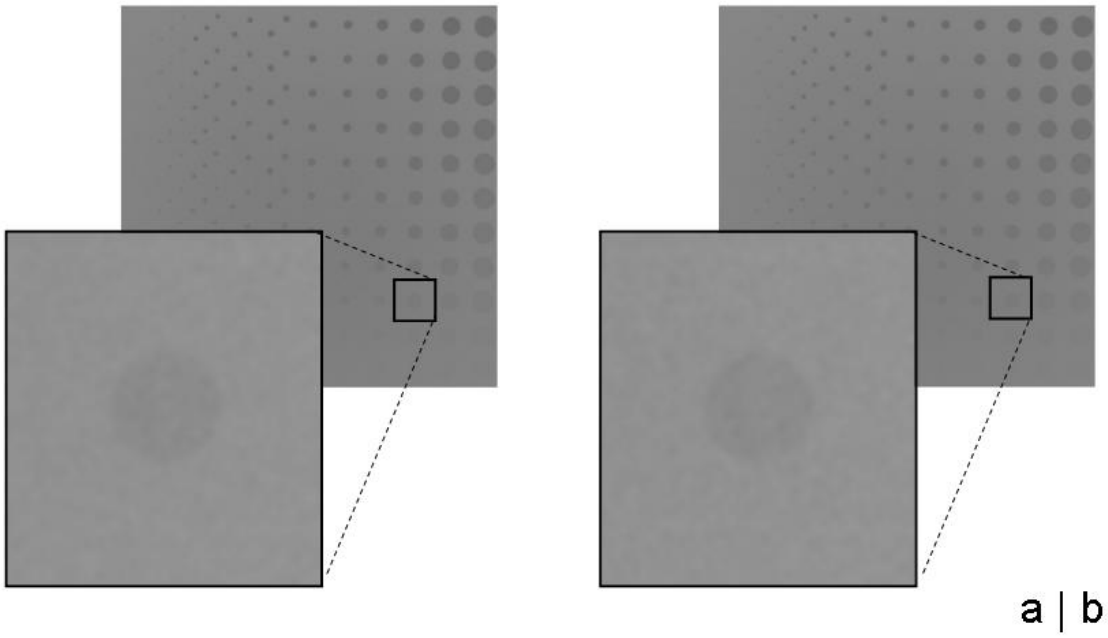

Figure 7 Zoomed detail of one of the holes in (a) the actual and (b) simulation images of burger phantom.

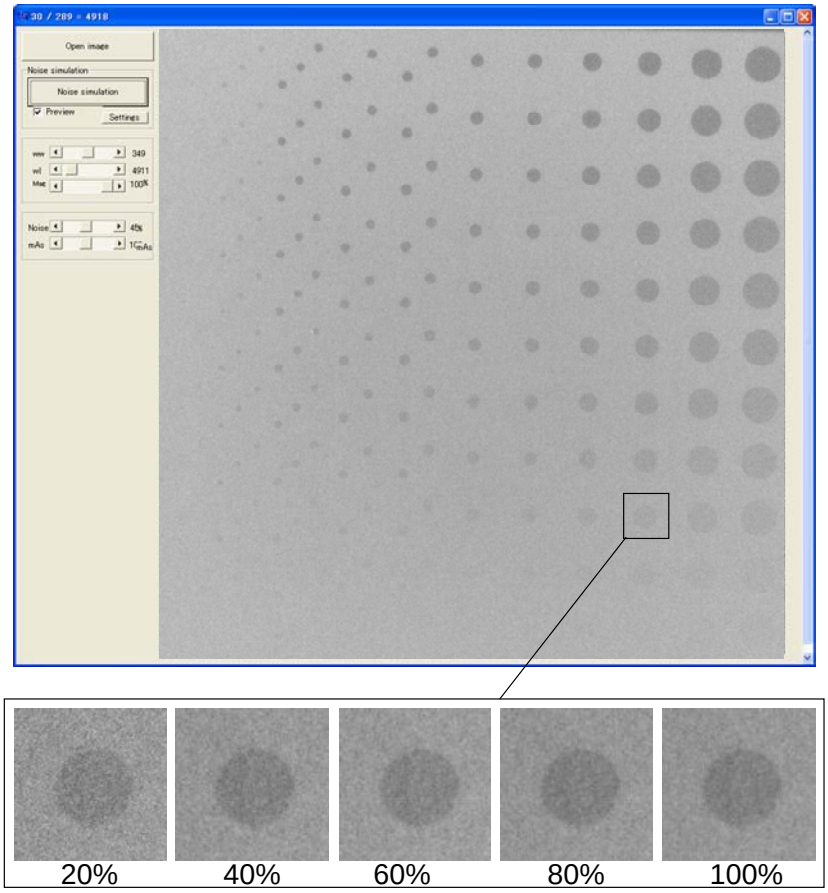

Figure 8 Graphical user interface (GUI) of our system (Upper) and simulation images (Lower). The percentages show incident quantum number (%) relative to the base image, *i.e.*, when a map of incident quantum numbers is multiplied by a weighting factor of 0.1, incident quantum number (%) becomes 10%.